geoconvention
Calgary • Canada • May 11-13 2026

A Petrophysical Model for the Duvernay Formation Through a Sequential Deterministic Workflow

Rafael Zambrano, Tyler Maksymchuk, Francisco Caycedo, Jesús Sierra
CAYROS Group Corp.

Summary

A sequential deterministic petrophysical workflow is presented for the estimation of mineral and pore-fluid volumes in the Duvernay Formation using a limited set of conventional open-hole logs. The workflow was developed and calibrated specifically for the Duvernay shale, with the objective of providing a practical methodology for petrophysical interpretation in an unconventional reservoir characterized by strong mineralogical variability, variable organic content, and a wide range of thermal maturity.

The workflow follows a step-by-step construction of the volumetric model. It begins with the estimation of mineral weight fractions and their normalization, followed by the calculation of matrix properties, porosity, kerogen volume, and formation fluid volumes. A final normalization of mineral and pore-fluid volumes is performed to ensure resolution of the volumetric model and internal consistency across all components.

Calibration of the workflow was performed using laboratory measurements from core material, including TOC from RockEval and LECO analysis, Petrophysical analysis from Gas Research Institute (GRI), Source Rock Analyzer (SRA) and Tight Rock Analysis (TRA) methods, and mineralogical analyses from X-Ray Diffraction (XRD) and X-Ray Fluorescence (XRF), complemented by nuclear magnetic resonance (NMR) and GR–induced spectroscopy logs (also known as Mineralogical logs) available in public database. While these datasets were used to condition and validate the model, the workflow itself relies only on typical triple-combo open-hole logs, allowing its application for the Duvernay across the basin where core data and advanced measurements are limited or unavailable.

Application of the workflow to multiple Duvernay wells shows that the main petrophysical properties can be estimated with a consistent level of confidence across different areas in the basin and maturity windows, using a reduced number of assumptions. These results demonstrate that when a sequential deterministic workflow is properly calibrated and constrained, can provide stable and meaningful petrophysical interpretations in complex unconventional shale systems.

Introduction

The Duvernay Formation is a Late Devonian organic-rich mudstone deposited within the Western Canada Sedimentary Basin (WCSB). It is widely regarded as the principal source rock for several conventional hydrocarbon accumulations in Alberta and more recently, as a major unconventional resource play. The formation was deposited in a marine basinal setting characterized by variable water depths, episodic anoxia, and significant lateral facies variability, resulting in pronounced heterogeneity in mineralogy, organic content, and reservoir quality.

Mineralogically, the Duvernay typically consists of varying proportions of carbonates (calcite and dolomite), siliceous components (quartz and feldspars), clay minerals (illite, chlorite and kaolinite), and pyrite. Total organic carbon (TOC) values commonly range between 2–8 wt%. Thermal maturity varies across the basin, transitioning from oil window to condensate and dry gas windows toward the west and northwest.

From a petrophysical perspective, the Duvernay presents several interpretation challenges. Porosity is low (often 3–8%), with contributions from interparticle, intraparticle, and organic-hosted pore systems. The presence of significant carbonate content can strongly influence bulk density and photoelectric factor responses, while high TOC intervals affect both density and neutron measurements. Additionally, pyrite and heavy mineral content can impact photoelectric factor-based mineral estimations. These complexities require careful calibration of mineral endpoints and TOC models, particularly when integrating triple-combo logs with core and XRD data.

This work focuses on wells located in the Kaybob, Edson–Willesden Green, and Innisfail areas of Alberta. These regions represent different depositional positions and maturity domains within the Duvernay fairway and display measurable variations in mineralogy, TOC distribution, and reservoir quality. By incorporating data from these areas, the proposed workflow has been assessed across a representative range of geological and petrophysical conditions within the play.

Database summary

A clear inventory of the core measurements and log datasets provides the foundation for selecting appropriate modeling strategies and assessing the robustness of the interpretations.

All data used in this work were retrieved from publicly available databases. The analysis is based on 17 wells located in the Kaybob, Edson–Willesden Green, and Innisfail areas of the Duvernay play. These wells represent a range of depositional and maturity conditions within the fairway and provide a representative dataset for evaluating the workflow.

All wells include a conventional triple-combo log suite acquired by different service providers. In addition, several wells contain advanced measurements such as nuclear magnetic resonance (NMR) and GR–Induced spectroscopy logs. Where available, these advanced logs were carefully reviewed and cross-checked against core measurements prior to incorporating their observations into the sequential deterministic workflow. This step ensured consistency between log responses and laboratory-derived properties before using the data to constrain the petrophysical model.

Core data is available for all wells included in this work. The laboratory dataset comprises mineralogical analyses (XRD and XRF), geochemical measurements (Rock-Eval and LECO TOC), and petrophysical core analysis (including GRI, SRA, and TRA). The integration of these routine and advanced core datasets provides the calibration points that strengthen the reliability of the log-based interpretations.

Data Challenges and Considerations

Log Quality and Consistency - Working with datasets acquired from multiple sources introduces inherent variability that must be carefully considered during interpretation. Differences between laboratories offering core measurements, particularly for analyses that require interpretive components such as XRD, are not uncommon. It is frequently observed that certain minerals are reported by some laboratories but not others, or that mineral fractions, especially within the clay group, vary between reports. These discrepancies may arise from differences in laboratory

protocols, analytical instrumentation, and data processing methodologies, including variations in mineral phase selection and quantification approaches.
Similar variability can be observed in well-log measurements acquired by different service providers. Even under comparable borehole conditions, differences in tool design, environmental corrections, calibration standards, and processing workflows can lead to measurable variations in log responses. These discrepancies tend to be more pronounced in advanced measurements such as NMR or GR–Induced spectroscopy logs. In addition to hardware and correction differences, variations in acquisition modes and tool settings, often driven by the objectives of the logging program, can further influence the recorded log responses. When working with data retrieved from public domain repositories, detailed metadata regarding acquisition parameters and laboratory procedures are not always available, making it more challenging to fully reconcile such differences. In contrast, these aspects are easier to track and control when working directly with operator-owned datasets. Recognizing and accounting for these sources of variability is therefore a crucial step in building a consistent petrophysical model.

Formation Heterogeneity - In addition to measurement variability, formation heterogeneity presents another important challenge. Differences in vertical resolution between core measurements and wireline logs are particularly relevant. Core analyses capture highly localized properties at the plug scale, whereas most conventional triple-combo logs represent an averaged response over a larger vertical interval.
During the data review, some core samples were observed to fall outside the general trends established by much of the dataset. In many cases, these deviations do not indicate measurement errors but instead reflect highly localized geological features that may not be representative of the broader interval. Because of the vertical resolution limitations of common logging tools, such isolated features may not be fully resolved in the log data.
Recognizing these localized events is important. While logs can capture most vertical variations observed in core, only a portion of these can be resolved with sufficient fidelity due to tool resolution constraints. Properly identifying and contextualizing these discrepancies helps prevent overfitting the model to isolated core measurements that are not log-resolvable.

There is no single formula to address all the challenges described above. However, acknowledging and carefully evaluating these factors is a critical step in the interpretation process. Insufficient data conditioning or overlooking these considerations can introduce bias and increase uncertainty in the petrophysical model. Although the detailed data preparation workflow is beyond the scope of this paper, the main challenges encountered during this work are highlighted here to provide context for the subsequent interpretation.

Mineralogical Data Analysis

The XRD dataset used in this work was compiled from eight different laboratories. Despite the multi-source origin of the data, the presence of the main mineral phases is consistent across all laboratories. The dominant minerals identified include quartz, feldspars, calcite, dolomite, and pyrite, while the clay fraction is primarily composed of illite. This consistency provides confidence in the overall mineralogical framework, even though minor variations in reported fractions are observed between laboratories, as discussed previously.

Pie charts summarizing the average mineral fractions derived from the XRD data for the Kaybob, Edson-Willesden Green and Innisfail areas illustrate the general mineralogical distribution within the study region.

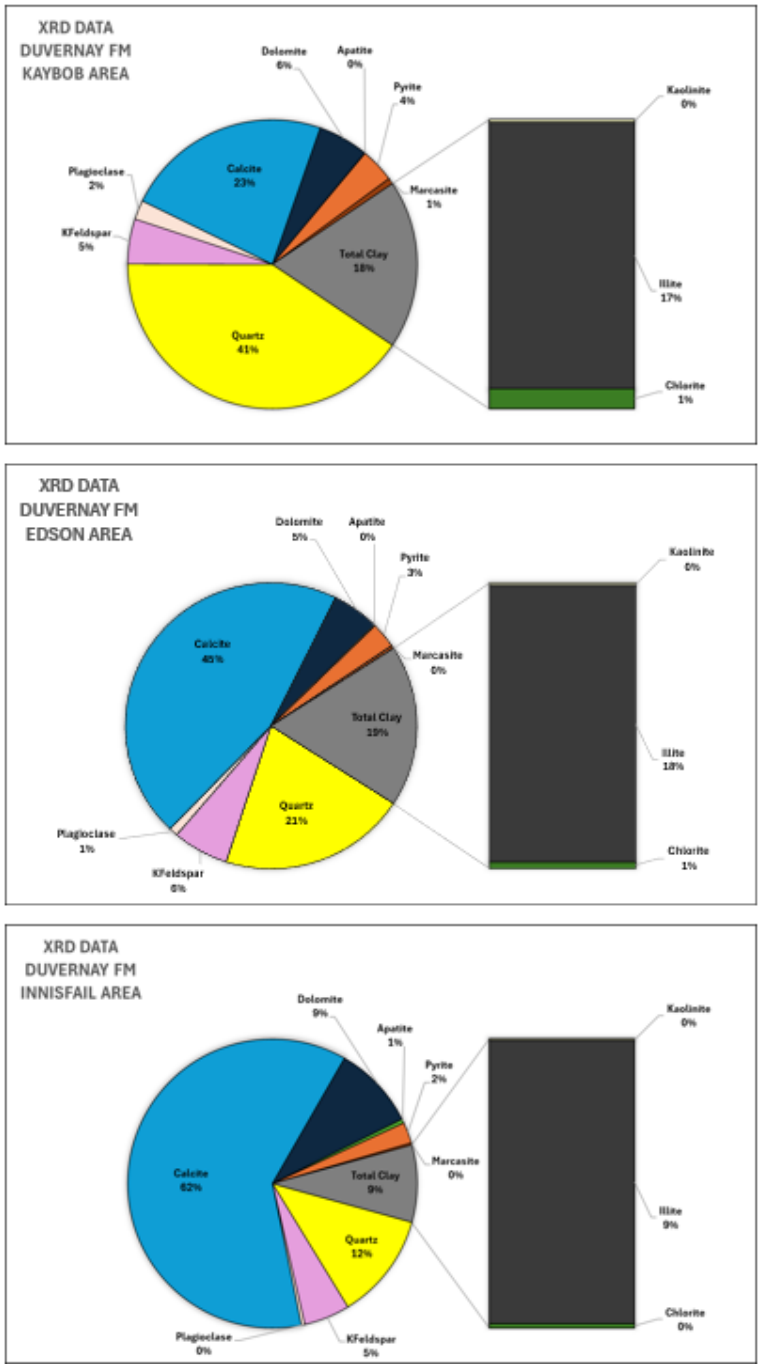


Figure 1. XRD mineral fractions average in Kaybob, Edson-Willesden Green and Innisfail areas.

As expected, variations are observed between areas, consistent with regional trends reported in the literature (e.g., Alberta Energy Regulator, 2016). In particular, the Innisfail area shows a higher proportion of carbonate minerals. These regional differences highlight the importance of understanding the geological context before constructing the mineral log model.

To better understand the stratigraphic context surrounding the Duvernay Formation, XRD data from adjacent formations, including the Ireton, Cooking Lake, and Majeau Lake, were also reviewed. Although the examination was not conducted with the same level of detail as for the Duvernay interval, it provided sufficient insight into mineralogical transitions across formation boundaries. This broader perspective helps explain variations in log responses and supports a more comprehensive interpretation of the study interval.

Mineral groups

The average mineral distributions derived from XRD serve as a practical guide for defining the mineral framework used in the log-based interpretation. Rather than attempting to model every individual mineral reported by XRD, the minerals were grouped into broader compositional families, namely Carbonate (CAR), Clay (CLA), and Quartz–Feldspar (QF). This grouping is motivated by two primary considerations.

First, the number of independent log measurements available in a typical triple-combo suite is insufficient to uniquely solve for all individual minerals identified by XRD. Attempting to invert for each mineral separately would lead to an underdetermined system and unstable solutions. By grouping minerals with similar log responses and geological behavior, the dimensionality of the system is reduced while preserving the dominant petrophysical controls.

Second, grouping ensures consistency across the multi-laboratory dataset. Since not all laboratories report the exact same set of mineral phases, focusing on the minerals that are consistently observed across all datasets allows the construction of a harmonized and robust mineral model.

This mineral simplification step is therefore not a loss of geological information, but rather a practical and necessary abstraction that enables a stable and interpretable log-based inversion.

Natural Mineralogical Pattern Associations in Organic-Rich Mudrocks

Organic-rich mudrocks commonly exhibit systematic mineralogical associations that reflect depositional environment, diagenetic evolution, and geochemical conditions, rather than random mixing of minerals. These patterns are not only conceptual interpretations; they can be directly observed in independent datasets such as XRD analyses and GR–induced spectroscopy logs, where consistent relationships between the different mineral components become evident across intervals and between wells.

Recognizing these recurring mineralogical associations is important for petrophysical interpretation. They provide geological justification for applying a constrained compositional model and help reduce the effective dimensionality of the mineral system without losing the dominant geological controls on log responses. In simple terms, instead of treating each mineral as completely independent, the model honors the natural relationships observed in the data.

By incorporating these natural associations into the workflow, the interpretation remains grounded in measurable geological trends, enabling robust first-order petrophysical solutions that are consistent with the depositional and diagenetic framework of the formation.

Empirical Carbonate-Clay Anti-Correlation

One of the most consistent and widely observed mineralogical associations in organic-rich mudrocks is the inverse relationship between carbonate and clay fractions. This anti-correlation is primarily controlled by sediment supply and dilution effects. Increased terrigenous input promotes clay accumulation while diluting carbonate deposition, whereas carbonate-rich intervals correspond to reduced siliciclastic influx.

In the Duvernay Formation and adjacent intervals, this carbonate–clay relationship is consistently observed in both XRD data and GR–Induced spectroscopy logs. The trend can be approximated using a simple empirical linear expression:

$$W_{CAR} = b - mW_{CLA}, \qquad (Eq.1)$$

For simplicity, the intercept is constrained to unity (b = 1), representing the limiting case in which clay content approaches zero and carbonate fraction approaches one within the simplified two-component framework. This representation provides a practical first-order approximation within the compositional range of the formation. The slope m represents the strength of the trade-off between carbonate and clay fractions and is determined from empirical fitting to mineralogical data (e.g., XRD or GR-induced spectroscopy). Observations from the compiled database indicate that m varies between areas. For example, the Kaybob area exhibits not only higher m values but also greater variability compared to the more southern regions. This reflects both a stronger and less uniform inverse relationship between carbonate and clay fractions in that area. For improved precision, the slope parameter should therefore be calibrated on an area-by-area basis.

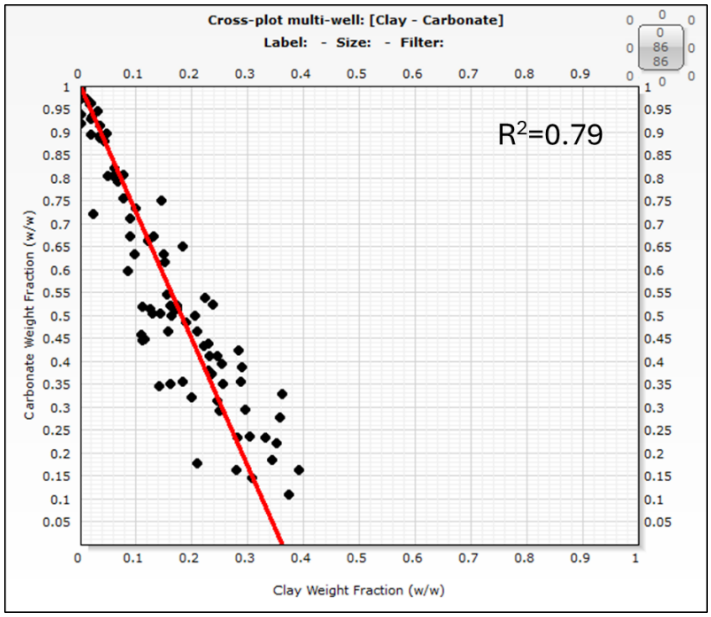


Figure 2. Cross-plot of XRD clay versus carbonate weight fractions showing the empirical inverse relationship observed across multiple wells in Edson-Willesden Green and Innisfail areas. The fitted linear trend (red line) captures the dominant carbonate–clay trade-off (R^2 = 0.79).

Similar carbonate–siliciclastic trade-off relationships have been documented in other unconventional shale systems, including the Eagle Ford, the Barnett, the Marcellus, and Vaca Muerta formations. These observations support the interpretation of the carbonate–clay trend as a depositional dilution effect rather than a purely statistical artifact.

It is important to emphasize that Eq. 1 does not represent a fundamental physical law, but rather a statistical approximation valid within the observed compositional domain of the formation. Its role is to reduce model dimensionality by linking carbonate and clay fractions while preserving the dominant geological trend evident in the data.

TOC and Pyrite Association

Total organic carbon (TOC) and pyrite content commonly exhibit a positive association in organic-rich mudrocks. Elevated TOC values typically reflect enhanced preservation of organic matter under low-oxygen to anoxic bottom-water conditions. These same conditions promote bacterial sulfate reduction, which in turn leads to the precipitation of iron sulfides, primarily in the form of pyrite. As a result, intervals enriched in organic carbon often show increased pyrite content.

This co-variation between organic carbon and pyrite has been documented in several sedimentary systems. Berner (1983) and Morse (1994) described the coupling between organic carbon accumulation and pyrite formation in normal marine siliciclastic sedimentary environments. Witkowsky (2012) reported a strong correlation between pyrite and TOC in the Haynesville Shale, noting that variations in the slope of the relationship may reflect differences in depositional conditions across the play. Similarly, Cuervo (2016) observed a correlation between TOC and pyrite weight fractions derived from advanced gamma-ray spectroscopy tools in the Vaca Muerta shale of Argentina.
In this work, the TOC – Pyrite association is approximated using a simple proportional relationship:

$$W_{PYR} = nTOC, \qquad (Eq. 2)$$

where the proportionality constant n represents the strength of the coupling between organic matter preservation and pyrite formation. As with the carbonate–clay relationship, this expression is empirical and should be calibrated to local data.

Although pyrite typically represents a minor volumetric component of the rock matrix, its presence is linked to TOC and can exert a disproportionate influence on certain log responses due to its relatively high density and strong photoelectric effect. Even small variations in pyrite content may therefore have measurable impacts on bulk density and photoelectric factor-based mineral estimations.

Sequential Deterministic Workflow

The workflow presented in this work follows a sequential deterministic approach, in which each component of the petrophysical model is solved independently and calibrated before progressing to the next stage. By constraining each stage independently, uncertainty propagation is controlled and diagnostic transparency is maintained. If discrepancies arise, they can be traced back to a specific stage of the workflow rather than being masked within a coupled inversion.

A schematic representation of the sequence is shown in Figure 3.

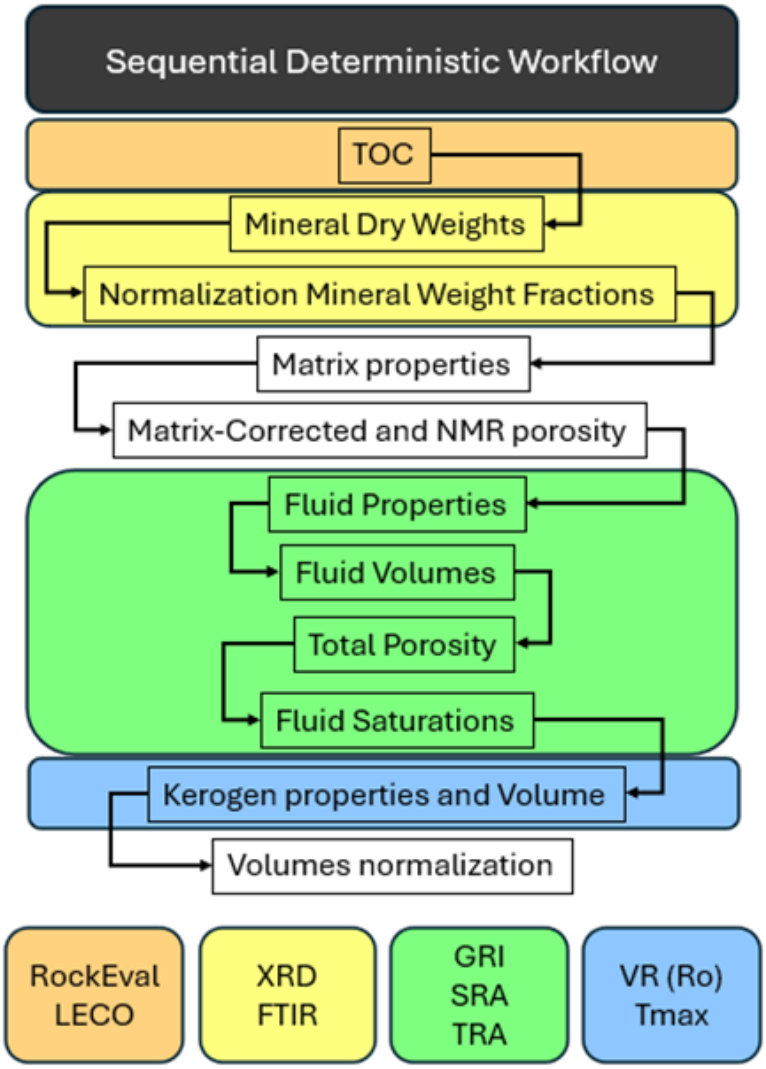


Figure 3. Conceptual framework of the proposed sequential deterministic workflow and associated core analysis constraints.

This structure allows each component of the model to be validated against independent measurements (e.g., core analysis, advanced logging measurements) prior to integration into the full volumetric solution.

It is important to emphasize that this paper does not detail the log data preparation stage. Prior to implementation of the workflow, logs were normalized, environmentally corrected where possible, and harmonized to ensure consistency across wells and logging service providers. Similarly, core analyses were reviewed, depth-matched to logs, and statistical outliers were removed prior to interpretation. Proper data conditioning is a prerequisite for any modeling approach and was completed before initiating the petrophysical evaluation.

Total Organic Carbon Estimation

Several commonly used log-based methods to estimate total organic carbon (TOC) were reviewed, including the DeltaLogR approach (Passey), uranium-based method, NMR-derived method, and the density method (Schmoker). In general, all these methods provided reasonable TOC estimates, although their performance varied. Some approaches showed better agreement with core data than others, with the NMR and density-based methods typically exhibiting stronger correlations.

For this workflow, the density method was selected mainly because of its simplicity and the ease with which it can be calibrated using core TOC measurements. Another practical advantage is that the density log (RHOB) is one of the most widely available measurements across the wells in the study area. The cross-plot shown below illustrates the relationship between the inverse of the RHOB log (x-axis) and core-measured TOC (y-axis). The cross-plot includes core samples from wells located in the Kaybob, Edson, and Innisfail areas.

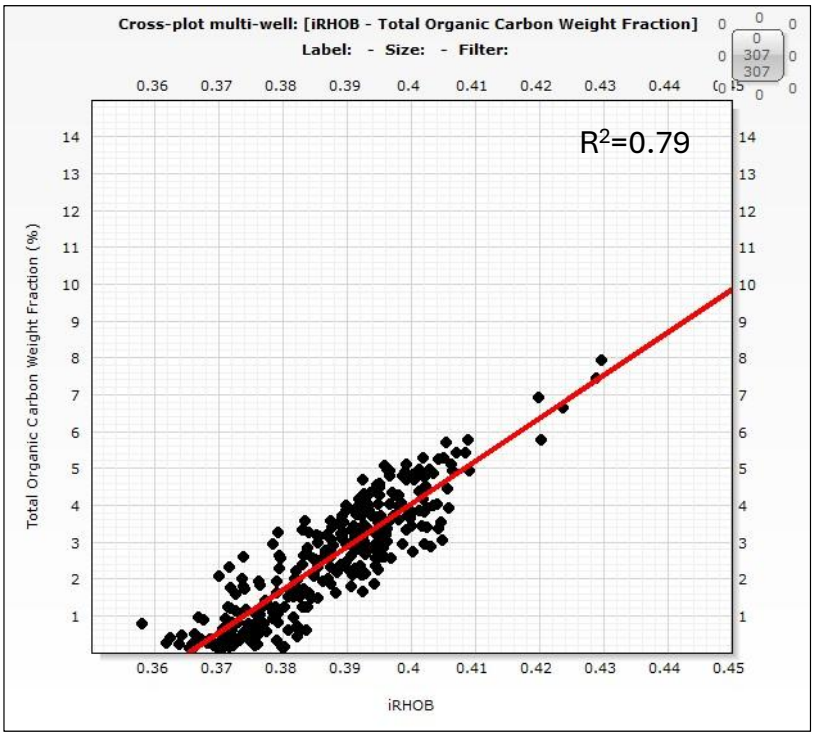


Figure 4. Multi-well cross-plot of inverse bulk density (iRHOB) and core-derived TOC weight fraction. The strong linear relationship (R^2 = 0.79) supports the use of the density-based approach for TOC estimation within the studied interval.

The density-based estimation of TOC relies on the fundamental contrast between the relatively low density of organic matter and the higher densities of the surrounding mineral matrix. As organic content increases, bulk density decreases, producing a measurable response in the RHOB log. By expressing the RHOB log in inverse form (1/RHOB), the relationship between RHOB and TOC becomes approximately linear over the compositional range of interest (J. Schmoker and T. Hester, 1983).

Using the multi-well calibration dataset described previously, a linear regression was performed between inverse RHOB (iRHOB) and core-measured TOC. The resulting empirical relationship is expressed as:

$$TOC = \frac{\left(116.2 \cdot \frac{1}{RHOB} - 42.4\right)}{100}, \qquad (Eq. 3)$$

where RHOB is in g/cc and TOC is expressed as weight fraction. The coefficients in this equation are derived from regression to the available core data (Figure 4) and therefore represent a formation-specific calibration for the studied intervals.

Other approaches could also be used at this stage. For example, machine-learning-based methods may yield more accurate TOC estimates, but they generally require more effort in terms of data preparation, log availability, and testing of different algorithms. Simpler alternatives, such as multiple linear regression, can also be effective. While they may not reach the performance of more advanced machine-learning models, they are easier to implement and tend to be more robust and transferable across datasets.

Estimation of Mineral Weight Fractions

Conventional deterministic petrophysical workflows typically begin by estimating mineral or rock volumes directly from log responses. In contrast, the sequential deterministic workflow proposed in this work first focuses on estimating mineral components in terms of weight fractions. This change in sequence is intentional and motivated by calibration considerations.

XRD data are reported in weight percent and therefore provide a direct and less subjective calibration framework when the mineral model is constructed in weight domain. By first solving mineral weight fractions, the interpretation remains closely tied to laboratory measurements before introducing additional assumptions required for volumetric conversion. This approach reduces ambiguity during the selection of log-to-mineral response endpoints and strengthens the geological consistency of the model.

It is important to recognize that wireline logs respond primarily to volumetric properties rather than weight fractions. However, once the mineral weight fractions are estimated, the corresponding volume fractions can be computed through density-based conversion. In this way, the workflow maintains consistency with log physics while benefiting from the direct comparability of weight fractions to XRD measurements.

Together with the TOC estimation, this step forms the core of the petrophysical model. A significant portion of the effort in this work has been devoted to ensuring that the mineral weight fractions are geologically consistent and statistically stable. In this context, access to reliable and representative XRD data is fundamental. Without robust mineralogical calibration data, the deterministic framework would lose much of its constraint and predictive capability.

To further ensure a fair representation of log responses associated with each mineral group, weighted-average log endpoints are calculated rather than adopting the default endpoint of a single predominant mineral. For example, instead of using the calcite endpoint to represent the

entire carbonate group, the effective endpoint is computed as a weighted average of calcite, dolomite, and other carbonate components. The weighting factors are derived from XRD data and represent the average mineral composition of the interval or area under evaluation.

This strategy explicitly accounts for compositional variability within mineral groups and reduces systematic bias in the mineral solution. Mineral endpoint values commonly used in conventional triple-combo log interpretation are well documented in the literature (e.g., Edmundson, 1979; Herron, 1993; logging service provider interpretation charts) and serve as the reference basis for constructing these weighted endpoints. It is important to note that mineral log endpoints reported in the literature may correspond either “dry” or to “wet” (bound-water-bearing) properties, particularly in the case of clay minerals. Care must therefore be taken to ensure internal consistency when selecting endpoint values, as mixing dry and wet properties can introduce systematic errors in the mineral solution. For the purposes of this workflow, dry mineral endpoint values are consistently used.

Carbonate and Clay Mineral Weight Fractions

Photoelectric factor (PEF) log is perhaps the best log candidate from the common triple combo suite to model the carbonate minerals (Calcite, Dolomite, Siderite) because of their high photoelectric factor values that can help discriminate from other mineral components. To use the PEF log in the Carbonate-Clay anti-correlation concept, the PEF log needs to become almost linear in carbonate weight fraction W_{CARB} through a closure condition, where all the components sum to 1:

$$W_{CAR} + W_{CLA} + W_{QF} + W_{PYR} = 1, \qquad (Eq.4)$$

Solving for W_{QF}:

$$W_{QF} = 1 - W_{CAR} - W_{CLA} - W_{PYR}, \qquad (Eq.5)$$

Rearranging the Eq. (1) to express clay as a function of carbonate:

$$W_{CLA} = \frac{1 - W_{CAR}}{m}, \qquad (Eq.6)$$

So, the W_{QF}:

$$W_{QF} = 1 - W_{CAR} - \frac{1 - W_{CAR}}{m} - W_{PYR}, \qquad (Eq.7)$$

The PEF log follows the linear volumetric mixing law, considering only the four mineral matrix components (CAR, CLA, QF and PYR), and because fluids and kerogen have low density and low photoelectric factor, their contribution is considered small, we can write explicitly as:

$$PEF \approx W_{CAR}P_{CAR} + W_{CLA}P_{CLA} + W_{QF}P_{QF} + W_{PYR}P_{PYR}, \qquad (Eq.8)$$

The W_x are wet weight fractions, no dry weight fractions as we are proposing here, nevertheless the difference is not relevant.

We substitute W_{CLA} and W_{QF} into Eq. 8:

$$PEF \approx W_{CAR}P_{CAR} + \frac{1 - W_{CAR}}{m} P_{CLA} + \left[1 - W_{CAR} - \frac{1 - W_{CAR}}{m} - W_{PYR}\right] P_{QF} + W_{PYR}P_{PYR}, \qquad (Eq. 9)$$

For interpretation purposes, Eq. 9 is algebraically rearranged by distributing and collecting terms to express the PEF as a linear function of carbonate weight fraction, with an explicit correction for pyrite. With this step we reformulate the equation into a form that is directly compatible with standard petrophysical cross-plot techniques:

$$PEF \approx W_{CAR}\left(\left(P_{CAR} - P_{QF}\right) - \frac{\left(P_{CLA} - P_{QF}\right)}{m}\right) + \left(P_{QF} + \frac{\left(P_{CLA} - P_{QF}\right)}{m}\right) + W_{PYR}\left(P_{PYR} - P_{QF}\right), \quad (Eq. 10)$$

By collecting the terms, we can see how the PEF is decomposed into three physically meaningful components:

A slop term that quantifies the sensitivity of PEF to changes in carbonate content,

$$A \equiv \left(P_{CAR} - P_{QF}\right) - \frac{\left(P_{CLA} - P_{QF}\right)}{m}$$

An intercept that represents the average contribution of non-carbonate background minerals (primarily clays and QF),

$$B \equiv P_{QF} + \frac{\left(P_{CLA} - P_{QF}\right)}{m}$$

And a pyrite correction term that accounts for the excess photoelectric response associated with pyrite relative to the background matrix,

$$C \equiv \left(P_{PYR} - P_{QF}\right)$$

So, Eq. 10 becomes the compact form:

$$PEF \approx AW_{CAR} + B + CW_{PYR}, \qquad (Eq. 11)$$

Neglecting the pyrite contribution we can say in this case the slope-intercept form defines the dominant carbonate trend:

$$PEF \approx AW_{CAR} + B, \qquad (Eq. 12)$$

In Eq. 12 the pyrite term is neglected as it is not important in the context of a correlation to the carbonate fraction. The objective is to show that the PEF is approximately linear with the carbonate weight fraction, so, we are trying to derive a carbonate proxy, for the moment, not a full mineral model. Pyrite will be managed later, through a different correlation.

Inverting for W_{CAR} from Eq.12, we get:

$$W_{CAR} \approx \frac{PEF - B}{A} = -\frac{B}{A} + \frac{1}{A} PEF, \qquad (Eq. 13)$$

Clay weight fraction is estimated through Eq. 6.

One of the main limitations of estimating W_{CAR} from the PEF log is its strong sensitivity to borehole conditions and to the presence of high-Z additives in the drilling mud. In many cases, the environmental corrections applied in the field by the logging service provider are insufficient to fully remove the influence of heavy additives such as barite. As a result, additional post-processing is often required, ranging from conventional approaches such as log normalization to more advanced techniques, including PEF log reconstruction using machine-learning-based methods.

Pyrite Weight Fraction

The modelling of the pyrite fraction in the petrophysical model is important due to the influence on the logs, in particular the RHOB log because of its high-density value (~5 g/cm^3). The lack of its characterization in the mineral log model impacts the grain density and therefore the porosity calculation.

A direct and more accurate estimation of pyrite fraction can be obtained from the GR–Induced spectroscopy logs thanks to its Sulphur fraction measurement. Nevertheless, those advanced logs are rarely acquired, and not available in all wells.

The cross-plot between previously computed TOC and pyrite weight fraction from XRD reveals a clear positive association across the compiled multi-well dataset. Although some scatter is present, the overall linear trend indicates that intervals enriched in organic carbon tend to contain higher pyrite content. This relationship is consistent with the depositional and diagenetic linkage between organic matter preservation and pyrite formation under reducing conditions. The regression fit shown in Figure 5 provides an empirical basis for approximating pyrite weight fraction as a function of TOC within the studied compositional range.

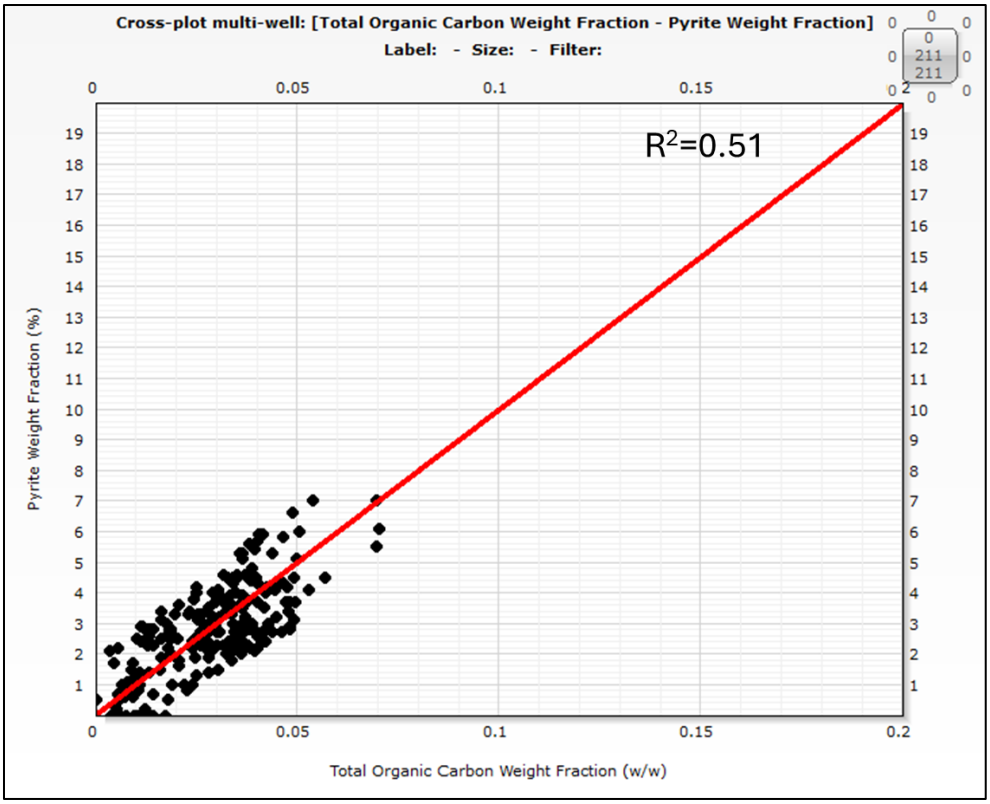


Figure 5. Multi-well cross-plot of TOC and pyrite weight fractions illustrating their positive association. The linear fit (red line) supports the empirical proportional relationship adopted in Eq. 14.

Despite its moderate relationship (R^2=0.51), the correlation is still useful to estimate the pyrite weight fraction. As the weight fraction usually remains small relatively to the contributions of the other components of the matrixes, the lack of accuracy should not significantly affect the model results.

Based on the regression analysis shown in the cross-plot, the slope of the relationship between pyrite and TOC approaches unity (≈ 0.996). For practical implementation within the workflow, this relationship is simplified as:

$$W_{PYR} = 1 \cdot TOC[w/w], \qquad (Eq. 14)$$

where both pyrite and TOC are expressed in weight fraction. This formulation implies that, on average within the calibration dataset, the pyrite weight fraction increases in direct proportion to TOC. In other words, intervals with higher organic content tend to contain comparable increases in pyrite content, reflecting their shared dependence on reducing depositional conditions.

It is important to emphasize that this expression is empirical and represents a first-order approximation valid within the compositional range of the studied dataset. The proportionality factor may vary between areas depending on local depositional and diagenetic conditions and therefore should be calibrated when sufficient data are available.

Quartz-Feldspars (QF) Weight Fraction

The Quartz–Feldspar (QF) group weight fraction is calculated by closing the matrix components to unity:

$$W_{QF} = 1 - W_{CAR} - W_{CLA} - W_{PYR}, \qquad (Eq. 15)$$

This formulation treats quartz and feldspars as a single siliceous group. The decision to merge these two minerals is both practical and petrophysically justified. From a log-response perspective, quartz and feldspars exhibit similar bulk densities and low photoelectric factors compared to carbonates and pyrite. Although minor differences exist, particularly in photoelectric factors due to compositional variations, their responses within a conventional triple-combo log suite are not sufficiently distinct to allow stable separation without introducing additional uncertainty.

Furthermore, XRD data across the study areas consistently shows the presence of both quartz and feldspars, although their relative proportions may vary. Grouping them reduces the dimensionality of the mineral system while preserving the dominant siliceous framework of the rock. Attempting to solve quartz and feldspar independently would increase the number of unknowns without providing additional independent log constraints.

At this stage, kerogen is not included in the equation or in the matrix model. The matrix (dry weight fraction) estimation has been calibrated against XRD analyses, which exclude organic matter from the measured mineral phases. Therefore, the summation in Eq. 15 is performed on the inorganic mineral components only.

This mineral modeling approach represents one of several practical solutions. At a local scale, more precise correlations may be established by integrating detailed core measurements or advanced log datasets with conventional triple-combo logs. Such approaches can yield higher resolution or more tightly calibrated results within a specific area.

However, the objective of this workflow is different. The intent is to develop a practical and transferable mineral model that can be applied at a broader scale across the Duvernay basin using a limited and commonly available log suite, minimal parameterization, and a clear physical understanding of the log responses. The emphasis is on geological consistency, robustness, and reproducibility rather than maximizing local precision.

In that sense, the model aims to be sufficiently accurate for basin-scale interpretation while remaining simple enough to be replicated and implemented efficiently across multiple wells.

Normalization of Mineral Weight Fractions

Before proceeding with subsequent petrophysical property computations, it is necessary to normalize the mineral weight fractions. This step ensures internal consistency of the mineral model and guarantees that the calculated mineral volumes remain physically meaningful.

In practice, the individual mineral weight fractions (w_i) obtained from the inversion or estimation process may not sum exactly to unity due to numerical approximations, rounding errors, or independent calculations performed for each mineral group. If these fractions are used directly,

the resulting volume fractions may be biased and could lead to inconsistencies in bulk property reconstruction.
To avoid this issue, the mineral weight fractions are first scaled using the total weight fraction:

$$S_{wf} = \sum_{i \in \{qf, car, cla, pyr\}} Wm_i \,, \qquad (Eq. 16)$$

where S represents the sum of all mineral weight fractions considered in the model (quartz–feldspar, carbonate, clay, and pyrite).

Each mineral volume is then computed as:

$$V_s = \sum_{i \in \{qf, car, cla, pyr\}} V_{iw} \,, \qquad (Eq. 17)$$

Where:

$$V_{iw} = \frac{Wm_i}{RHOm_i \cdot S_{wf}}, \qquad (Eq. 18)$$

This step is essential because petrophysical logs respond primarily to volumetric properties rather than mass fractions. Without normalization, small deviations in total weight could propagate into errors in RHOB reconstruction, PEF matching, and subsequent porosity and fluid calculations.
By harmonizing the mineral fractions at this stage, the workflow ensures that all later computations are based on a physically consistent and properly scaled mineral framework.

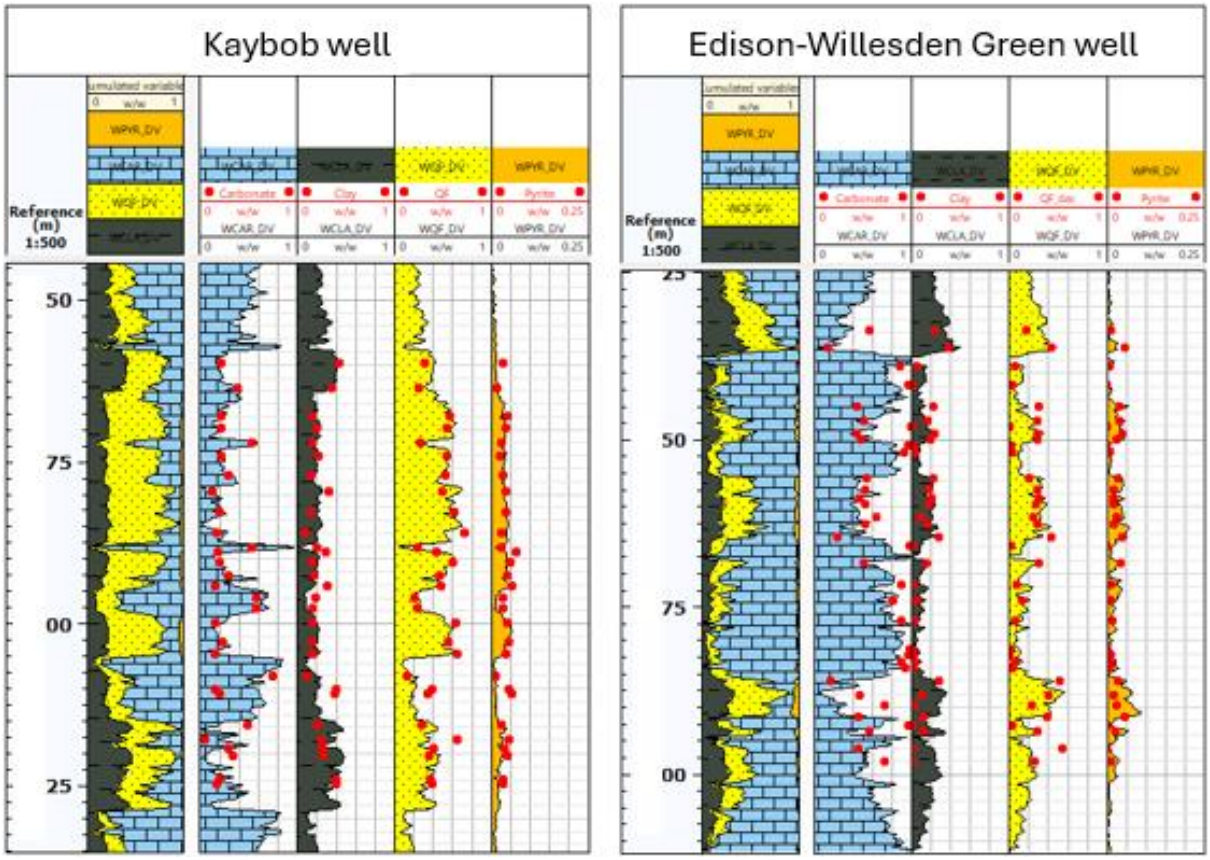


Figure 6. Comparison between normalized mineral log results and XRD measurements (red dots) for representative wells from the Kaybob and Edson-Willesden Green areas. The agreement illustrates the consistency achieved after normalization of mineral weight fractions.

Matrix-Derived Properties and Corrected Porosity

From the mineral log model, matrix properties such as matrix density ($RHOMA$) and matrix thermal neutron response ($TNMA$) can be derived. These properties represent the effective lithological response of the inorganic matrix and are computed from the estimated mineral weight fractions.

The matrix density is calculated as:

$$RHOMA = \frac{\Sigma_i Wm_i}{\Sigma_i \frac{Wm_i}{RHOm_i}}, \qquad (Eq.19)$$

Similarly, the matrix thermal neutron response (in limestone scale) is obtained as:

$$TNMA = \frac{\Sigma_i \frac{Wm_i}{RHOm_i} TNm_i}{\Sigma_i \frac{Wm_i}{RHOm_i}}, \qquad (Eq.20)$$

where ($\mathrm{RHO}m_i$) and (TNm_i) correspond to the mineral density and thermal neutron values for each mineral component, respectively. These mineral endpoints are determined using weighted averages within each mineral group to reflect compositional variability.

Core Grain Density Considerations

Routine core analysis (RCAL) grain density measurements may not always remove organic matter prior to analysis. If organic matter is not removed or properly accounted for, it is included in the measured "grain" volume while contributing less mass than the inorganic minerals, resulting in an artificially lower grain density.

For quality control and fair comparison with matrix density computed from the mineralogical model (RHOMA), the measured core grain density should be corrected for the presence of organic matter. This correction can be performed using a solid-mixture relationship:

$$RHOG = \frac{1 - \frac{TOC}{\chi_{om}}}{\frac{1}{RHOG_{core}} - \frac{\left(\frac{TOC}{\chi_{om}}\right)}{\rho_{om}}}, \qquad (Eq.21)$$

This correction ensures consistency between laboratory and log-derived matrix properties.

Matrix-Corrected Porosity

The computed matrix properties ($RHOMA$ and $TNMA$) are then used to derive matrix-corrected porosities from the RHOB and neutron porosity in limestone matrix (NPHIL) logs. This step removes the lithological influence from the porosity response, isolating the fluid-related contribution.

The matrix-corrected density porosity is calculated as:

$$DPHI_{MC} = \frac{RHOMA - RHOB}{RHOMA - 1}, \qquad (Eq.22)$$

and the matrix-corrected neutron porosity as:

$$NPHI_{MC} = \frac{NPHIL - TNMA}{1 - TNMA}, \qquad (Eq.23)$$

These corrected porosities provide a more representative estimate of pore volume by accounting for variations in mineral composition. However, it is important to recognize that kerogen is not included in the inorganic matrix model used to derive RHOMA and TNMA. Consequently, the matrix-corrected porosities still retain influence from organic matter.

Fluid Indication from Corrected Porosity Logs

In conventional reservoirs, a quick-look fluid indication often relies on neutron–density crossover. However, in unconventional reservoirs with complex mineralogy, the raw limestone-scale logs (NPHIL and DPHI_LIM) frequently fail to show a clear crossover due to strong lithological effects. As discussed by Mosse et al. (2016), the combination of matrix-corrected porosities (DPHI_MC and NPHI_MC) provides a more reliable qualitative indicator of fluid type in unconventional

reservoirs. When lithological effects are removed, crossovers between corrected porosities become more evident and can be interpreted in terms of fluid phase.

Figure 7 presents examples from the Kaybob area spanning gas, condensate, and oil windows. In each well, the first track displays the estimated mineralogy from the workflow. The second track shows the raw density and neutron porosity logs (limestone matrix). The third track presents the matrix-corrected density and neutron porosities. The yellow shading between DPHI_MC and NPHI_MC highlights intervals where crossover occurs, typically associated with the presence of lighter hydrocarbon phases.

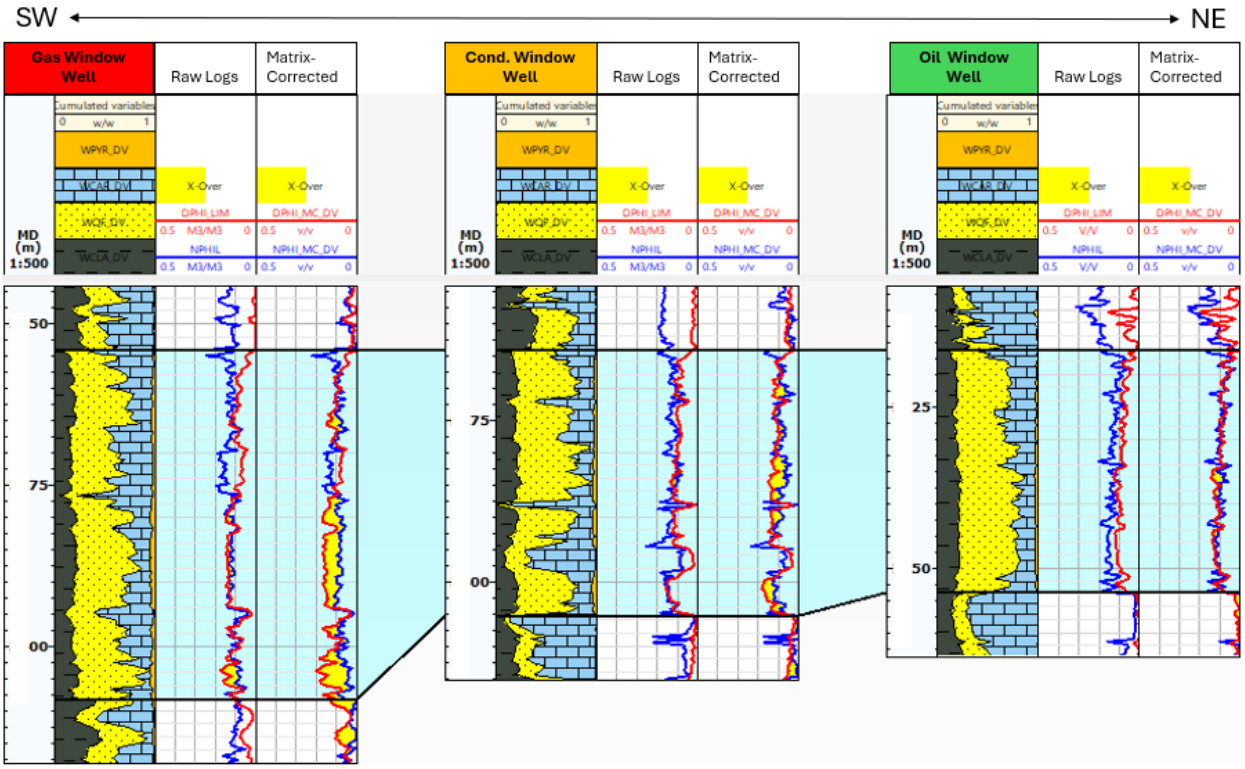


Figure 7. Example wells along a SW–NE transect in Kaybob area. Raw versus matrix-corrected porosity logs illustrating enhanced fluid indication across maturity windows.

Although the matrix-corrected porosities do not explicitly remove the influence of kerogen, this limitation is shared with the raw neutron and density logs. Therefore, the observed crossover between DPHI_MC and NPHI_MC is not primarily controlled by mineralogical variations or organic content, but rather by the presence of light hydrocarbons. In other words, once the inorganic lithological effects are removed, the remaining divergence between the porosity curves predominantly reflects fluid type.

NMR Porosity

Nuclear Magnetic Resonance (NMR) porosity plays a critical role in evaluating the storage potential of unconventional shale reservoirs. In this workflow, NMR porosity is interpreted primarily as representing the inorganic matrix-hosted pore system, including interparticle porosity and clay-associated pores containing clay-bound water (CBW).

Unlike conventional porosity logs, NMR measurements respond directly to hydrogen in fluids occupying pore space and are insensitive to mineral matrix effects. In organic-rich systems, this is particularly important because NMR is far less influenced by the hydrogen index of solid kerogen compared to neutron porosity logs. As a result, NMR provides a more reliable estimate of porosity associated with inorganic pore networks.

Although NMR is not always available in every well, it should ideally be included in the logging suite when evaluating unconventional shales. Within this workflow, NMR porosity is considered a key input. However, recognizing that this measurement may be absent in some wells, an alternative estimation approach is proposed.

A strong empirical relationship was observed between measured NMR total porosity and a combination of thermal neutron porosity in limestone matrix (NPHIL) and compressional slowness (DTC). This relationship can be expressed as:

$$MPHIR = -0.04 + 0.037\,NPHIL + 0.00034\,DTC, \qquad (Eq.\,24)$$

The cross-plot below compares measured NMR porosity from different logging service providers with NMR porosity estimated using the regression ($MPHIR$) above. The resulting correlation coefficient (R ≈ 0.77) indicates good agreement, supporting the use of this empirical relationship where direct NMR measurements are unavailable.

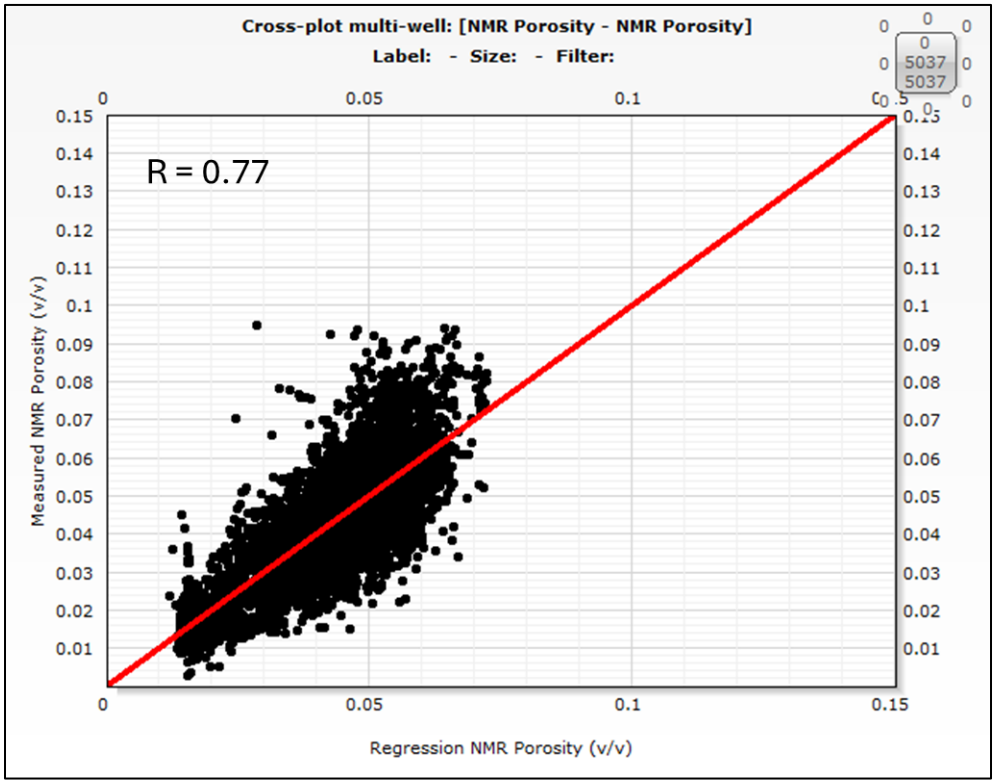


Figure 8. Cross-plot of measured NMR porosity versus regression-estimated NMR porosity (MPHIR) across multiple wells. The correlation coefficient (R = 0.77) indicates good agreement between measured and predicted values.

It is important to note that NMR responses may vary slightly depending on tool design and acquisition configuration. Therefore, although the proposed regression provides a practical substitute when NMR data is unavailable, direct NMR measurements should always be preferred whenever possible. Within this workflow, the regression-based estimate is optional and intended as a fallback solution rather than a replacement for measured NMR data. For simplicity in subsequent calculations and explanations, the term $MPHIR$ will be used consistently to denote NMR porosity, whether obtained from direct measurement or from the regression-based estimate.

Fluids and Porosity Model

Once the mineral framework and matrix-corrected porosities have been established, the next step is to estimate fluid volumes and total porosity. The workflow used in this work separates the problem into two interconnected components: the water model and the hydrocarbon model. Together, these components define the distribution of fluids within the pore system and ultimately determine total porosity.

Water Model

The water model begins with the estimation of formation water resistivity (Rw). Salinity is first used to calculate Rw at surface conditions, which is then corrected to reservoir temperature.

With Rw defined, Archie's formulation is applied to estimate the water-filled porosity ($PHIW$). In this workflow, Archie's relationship is expressed using an effective exponent parameter (MN), representing the tortuosity of the water phase within the pore system, rather than treating the cementation exponent (m) and saturation exponent (n) separately. Physically, MN incorporates the influence of the cementation exponent (m), which reflects pore geometry, and the saturation exponent (n), which describes the distribution of water within the pore network. A similar representation is discussed in dielectric-based formulations of water-phase tortuosity.

Although Archie's law was originally developed for clean sandstones, it remains widely applied in organic-rich mudrocks as a first-order resistivity framework when properly calibrated. For practical implementation, MN is treated as a formation-calibrated effective exponent governing the resistivity–porosity relationship:

$$PHIW = \left(\frac{Rw}{Rt}\right)^{\frac{1}{MN}}, \qquad (Eq.25)$$

The effective water-phase tortuosity exponent (MN) is calibrated by comparing resistivity-derived water-filled porosity ($PHIW$) with independent porosity measurements, primarily NMR porosity, in intervals interpreted as predominantly water-bearing. In such intervals, water-filled porosity is expected to approximate total inorganic porosity, providing a physically consistent reference for adjusting MN. This calibration ensures that the resistivity–porosity relationship remains consistent with measured pore volume while maintaining a stable and transferable parameter for basin-scale application.

A clean water zone is not clearly identifiable within the Duvernay Formation. The underlying Ireton Formation, which is regionally adjacent and shares comparable burial and thermal history, was therefore used as an initial reference interval for calibration. This approach provides a starting constraint for MN and Rw; however, final parameter selection was validated within the Duvernay through comparison with independent porosity measurements and core-derived water saturation.

Based on this calibration strategy, an MN value near 2 provided the most consistent agreement across the evaluated wells.

The resistivity-derived water-filled porosity ($PHIW$) primarily reflects water occupying the inorganic pore network. Organic-hosted porosity within kerogen is assumed to contribute negligibly to the connected conductive phase under the maturity conditions considered.

In addition, the water hydrogen index (HI_w) is computed as a function of salinity using the relationships described by Gaymard and Poupon (1968). This parameter is required for consistent hydrogen-index scaling in the hydrocarbon model.

Hydrocarbon Model

The hydrocarbon model builds on NMR porosity ($MPHIR$). In this workflow, $MPHIR$ represents the hydrogen-filled porosity of the inorganic matrix and may be obtained either directly from the measured NMR log or, when unavailable, from the regression-based estimate described earlier. Because NMR primarily responds to hydrogen in pore fluids and is largely insensitive to lithology, it provides a reliable reference for fluid partitioning within the inorganic pore system.

To isolate the hydrocarbon contribution, the hydrogen-equivalent water-filled portion ($PHIW \cdot HI_w$) is first removed from $MPHIR$. The remaining hydrogen response is then scaled by the hydrocarbon hydrogen index (HI_{hc}) to recover the hydrocarbon-filled pore volume:

$$PHIHC = \frac{MPHIR - PHIW \cdot HI_w}{HI_{hc}}, \qquad (Eq.26)$$

The inverse scaling with the hydrocarbon hydrogen index (HI_{hc}) compensates for the lower hydrogen density of hydrocarbons relative to water. In gas-bearing intervals, where HI_{hc} is small, the NMR response under-represents the true pore volume; dividing by HI_{hc} restores the actual hydrocarbon-filled porosity.

The HI_{hc} is estimated from hydrocarbon density, which varies with fluid type (oil, condensate, or gas window conditions), following the relationships described by Gaymard and Poupon (1968).

This formulation ensures that the separation of water and hydrocarbon volumes remains physically consistent with the hydrogen-index response of the measurement, while maintaining compatibility with the sequential deterministic framework.

Total Porosity

Once the water-filled and hydrocarbon-filled porosities are determined, total porosity is obtained as:

$$PHIT = PHIW + PHIHC, \qquad (Eq.27)$$

The resulting total porosity primarily represents the inorganic matrix-hosted pore system as measured by NMR. Organic-hosted porosity within kerogen is not explicitly included in this term. Although kerogen volume is estimated from TOC using maturity-dependent kerogen properties, the transformation of kerogen volume into organic pore volume requires additional calibration data that are not available for the wells included in this work. Quantification of organic-hosted porosity typically relies on specialized core analyses such as Focused Ion Beam–Scanning Electron Microscopy (FIB-SEM), Field-Emission Scanning Electron Microscopy (FE-SEM), and gas

adsorption measurements (N_2/CO_2), which are among the most effective methods for characterizing pore types and pore size distributions in shales.
Given the limited availability of such calibrated datasets, the present workflow focuses on the inorganic pore system for basin-scale deterministic evaluation, while acknowledging that incorporation of organic-hosted porosity represents a potential extension of the petrophysical model.

Kerogen computation
Within the sequential deterministic workflow, kerogen is intentionally incorporated after the mineral matrix and fluid volumes have been established. This ordering is deliberate.
The mineral model is first solved in terms of inorganic matrix components using XRD-calibrated weight fractions. This ensures that the inorganic framework is geologically constrained and consistent with laboratory measurements. Since XRD mineralogy excludes organic matter, solving the mineral system independently avoids circularity and prevents kerogen from biasing the matrix solution.
Similarly, fluid volumes are estimated using NMR-derived porosity and resistivity-based water volume calculations, both of which primarily represent pore-hosted fluids within the inorganic matrix.
Only after the mineral and fluid systems are defined is kerogen introduced. At this point, total organic carbon (TOC) has already been estimated from density-based methods, and the remaining step is to convert this mass-based measurement into a volumetric kerogen fraction. This sequential approach maintains physical consistency and avoids overparameterization of the mineral solution.

From TOC to Kerogen Volume
TOC is defined as the mass fraction of organic carbon (M_{Corg}) relative to the total rock mass (M_{ma}):

$$TOC = \frac{M_{Corg}}{M_{ma}}$$

However, petrophysical modeling requires kerogen volume rather than carbon mass fraction. Therefore, a transformation from carbon mass to kerogen volume must be performed.
The total mass of kerogen (M_k) relates to carbon mass through the carbon mass fraction of kerogen (C_k):

$$TOC = \frac{M_k \cdot C_k}{M_{ma}}$$

Expressing mass in terms of density and volume:

$$TOC = \frac{\phi_k \cdot \rho_k \cdot C_k}{\rho_{ma} \cdot \phi_{ma}}$$

Solving for kerogen volume fraction (ϕ_k):

$$\phi_k = \frac{TOC \cdot \rho_{ma} \cdot \phi_{ma}}{\rho_k \cdot C_k}$$

In practical implementation within the workflow, the kerogen volume fraction ($VKER$) is expressed as:

$$VKER = \frac{TOC \cdot RHOMA \cdot (1 - PHIT)}{Rhok \cdot Ck}, \qquad (Eq. 28)$$

The term $(1-PHIT)$ represents the solid (non-porous) fraction of the rock matrix in which kerogen resides.

Estimation of Kerogen Properties

Kerogen properties are not constant. Both kerogen density ($Rhok$) and carbon mass fraction (C_k) vary systematically with maturity (Ro%).

Craddock et al. (2019) describes empirical relationships to estimate these parameters as functions of thermal maturity. By incorporating maturity-sensitive kerogen properties, the workflow accounts for the evolving nature of organic matter rather than treating kerogen as a fixed-density component.

Weights to Volumes Conversion and Normalization

The final operation in the sequential model is the transformation of matrix-referenced mineral weights into volumetric fractions of the formation. This requires scaling the mineral components to the solid portion of the rock and applying a normalization step to ensure that all formation constituents sum to unity.

$$V_{iv} = \frac{(1 - PHIT - VKER) \cdot \frac{V_i w}{Vs}}{S_v}, \; Vker = \frac{VKER}{S_v}, \qquad (Eq. 29)$$

Where:

$$S_v = \sum_{i \in \{car,\, cla,\, qf,\, pyr\}} \left[(1 - PHIT - VKER) \cdot \frac{V_{iw}}{V_s}\right] + VKER + PHIT, \qquad (Eq. 30)$$

The volumetric normalization described above represents the last step in the sequential deterministic workflow and ensures full internal consistency of the mineral, kerogen, and fluid components. By converting mineral weight fractions into formation-based volume fractions and enforcing strict volumetric closure, the model guarantees that all formation constituents, minerals, kerogen, and pore fluids sum to unity. This step is not merely mathematical; it reconciles independently estimated domains into a physically coherent representation of the rock.

Throughout the workflow, each component is solved in sequence: mineral composition constrained by XRD, inorganic porosity derived from NMR, fluid partitioning governed by resistivity and hydrogen-index physics, and kerogen volume estimated from TOC with maturity-dependent properties. The final normalization integrates these elements into a single volumetric

framework, preserving their independent calibrations while ensuring compatibility within the overall formation balance.

This structured approach is particularly important in organic-rich mudrocks, where multiple coupled domains, minerals, fluids, and kerogen, interact in complex ways. By solving each domain independently before enforcing volumetric closure, the workflow minimizes parameter interdependence, reduces circularity, and maintains geological interpretability. The result is a robust and transferable petrophysical model suitable for basin-scale evaluation while remaining grounded in measurable physical relationships.

Figures 9 and 10 present the complete output of the sequential deterministic workflow for two representative wells: one from the Kaybob area and one from the Edson-Willesden Green area. The figures illustrate the progression from raw log measurements to the final volumetric model, allowing direct comparison between log-derived properties and core data at each stage of the workflow.

Tracks 1 through 5 display the raw log measurements used as inputs to the workflow, including Gamma Ray (GR), Photoelectric Factor (PEF), Neutron Porosity in Limestone matrix (NPHIL), Bulk Density (RHOB), Compressional Slowness (DTC), and Deep Resistivity (RESD). These logs constitute the conventional triple-combo dataset augmented with sonic and resistivity measurements, forming the foundation of the deterministic interpretation.

Track 6 presents the mineral log model expressed in weight fractions. The four derived mineral groups Clay (WCLA), Quartz–Feldspar (WQF), Carbonate (WCAR), and Pyrite (WPYR) are shown in cumulative format. By construction, the mineral weight fractions are normalized to sum to unity, ensuring internal consistency of the dry mineral framework.

Track 7 shows the grain density derived from the mineral log model (RHOMA) plotted in black. Core grain density measurements are shown as red dots, along with the same samples corrected for organic matter content (green dots). The agreement between modeled and corrected core grain density demonstrates the consistency of the mineral framework.

Track 8 compares total organic carbon (TOC) estimated from the calibrated density-based method with core TOC measurements, illustrating the robustness of the TOC calibration across intervals with varying organic content.

Track 9 displays total porosity derived from the petrophysical model alongside core porosity measurements, providing validation of the inorganic porosity estimation.

Track 10 shows the resistivity-derived water-filled porosity (PHIW) in blue compared with NMR porosity (green curve). In intervals interpreted as predominantly water-bearing, the convergence of these curves reflects the calibration of the effective exponent (MN).

Track 11 presents water saturation estimated from the petrophysical model together with core-derived water saturation values, further supporting the calibration of the resistivity framework.

Track 12 displays the fully integrated volumetric model in cumulative format, including all mineral components, kerogen volume, and pore-fluid volumes (hydrocarbons and water). This track represents the final output of the sequential deterministic workflow after volumetric normalization and closure.

Together, these figures illustrate the internal consistency of the workflow and the agreement between log-derived properties and independent core measurements across different geological settings within the Duvernay play.

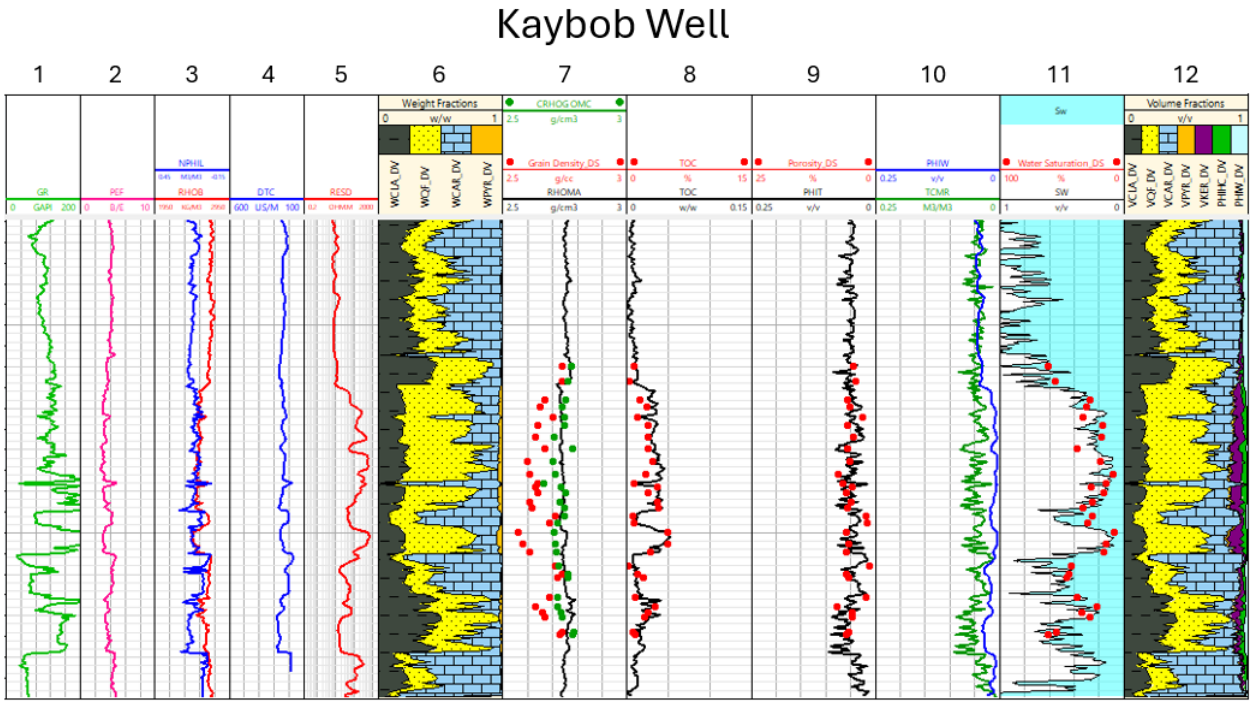


Figure 9. Application of the sequential deterministic workflow to a representative Kaybob well. The figure shows raw logs (Tracks 1–5), mineral weight fractions (Track 6), modeled and core grain density (Track 7), TOC comparison (Track 8), total porosity validation (Track 9), resistivity-derived water-filled porosity versus NMR porosity (Track 10), water saturation comparison (Track 11), and the final volumetric model including minerals, kerogen and pore fluids (Track 12).

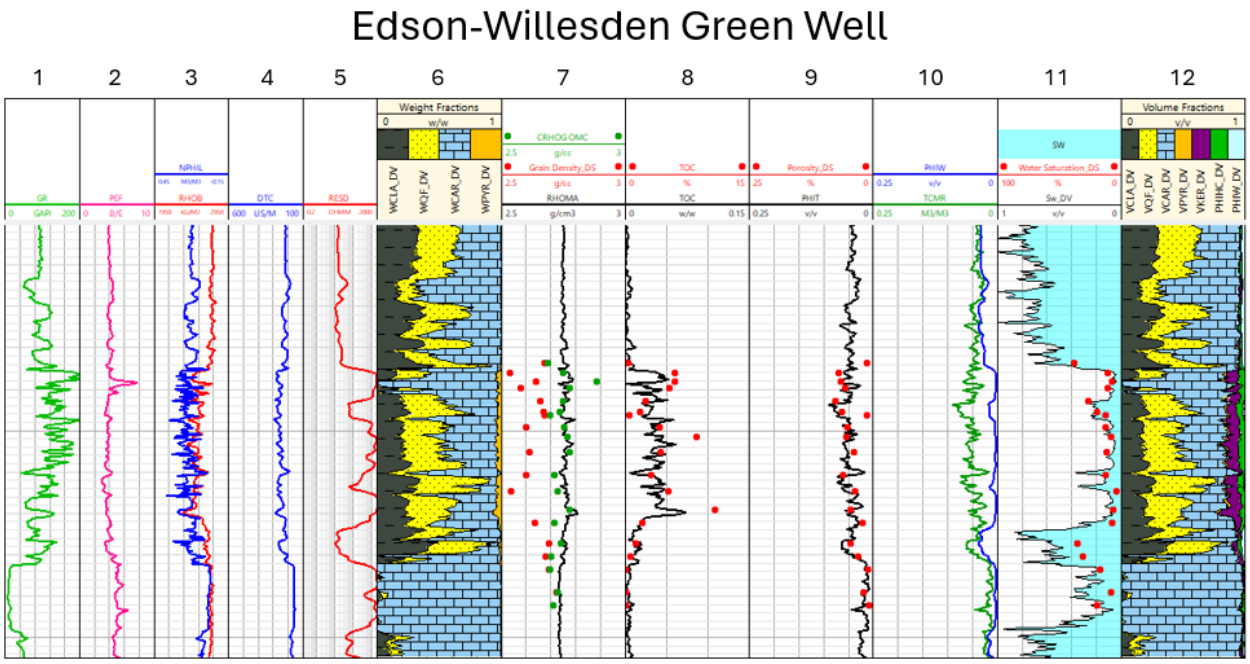


Figure 10. Application of the sequential deterministic workflow to a representative Edson-Willesden Green well. The full interpretation sequence is displayed from raw log inputs to the final volumetric model, illustrating consistency of mineral, porosity, and fluid estimates across a different area of Duvernay Formation.

Conclusions

A sequential deterministic petrophysical workflow has been developed for the Duvernay Formation to estimate mineral composition, inorganic porosity, kerogen volume, and fluid distribution using a limited suite of conventional open-hole logs. While individual petrophysical properties may be computed through alternative approaches, the principal contribution of this work lies in the structured, stepwise framework used to build the volumetric model.
Each domain (minerals, matrix properties, porosity, fluids, and kerogen) is solved and calibrated independently before integration. This sequential structure reduces parameter interdependence, limits ambiguity propagation, and preserves geological interpretability. By constraining each stage with laboratory measurements and log physics prior to progressing to the next, the workflow maintains internal consistency and transparency.

Although developed specifically for Duvernay Formation, the methodology is transferable to adjacent formations through appropriate mineralogical adjustments. The results demonstrate that a disciplined sequential deterministic framework, when properly calibrated and harmonized, provides stable and physically grounded petrophysical interpretations in complex organic-rich shale systems using conventional log data.

List of Symbols

Wm_i - Dry weight fraction each mineral i, (w/w)
$\mathrm{RHOm_i}$ - Density of dry mineral I, (g/cc)
TNm_i - Thermal neutron value of dry mineral i in limestone matrix, (v/v)
χ_{om}- Carbon mass fraction in the organic matter
ρ_{om}- Density of organic matter, (g/cc)
ρ_k - Kerogen density, (g/cc)
ρ_{ma} - Matrix density, (g/cc)
S_{wf} - Weight normalization factor
V_{iw} - Intermediate mineral volume each mineral i (weight-to-volume conversion)
V_s - Sum of intermediate volumes
V_{iv} - Final mineral volume fraction each mineral i
S_v - Volumetric normalization factor
W_{CAR} - Carbonate dry weight fraction, (w/w)
W_{CLA} - Clay dry weight fraction, (w/w)
W_{PYR} - Pyrite dry weight fraction, (w/w)
W_{QF} - Quartz-Feldspar dry weight fraction, (w/w)
P_{CAR} - PEF value for the carbonate group mineral, (b/e)
P_{CLA} - PEF value for the clay group mineral, (b/e)
P_{QF} - PEF value for the quartz-feldspar group mineral, (b/e)
P_{PYR} - PEF value for pyrite mineral, (b/e)

References

Responses of neutron and formation density logs in hydrocarbon bearing formations, R. Gaymard and A. Poupon, 1968.
Sedimentary pyrite formation: and update, R. Berner, 1983.
Organic Carbon in Bakken Formation, United States Portion of Williston Basin, J. Schmoker, 1983.
What determines sedimentary C/S ratios?, J. Morse and R. Berner, 1994.
Predicting Pyrite and Total Organic Carbon from Well Logs for Enhancing Shale Reservoir Interpretation, J. Witkowsky et al., 2012.
Application and Quality Control of Core Data for the Development and Validation of Elemental Spectroscopy Log Interpretation, Herron et al., 2014.
Fluid typing and maturity index from logs: A new framework for petrophysical evaluation of organic-rich mudrock, L. Mosse et al., 2016.
Towards a Simplified Petrophysical Model for the Vaca Muerta Formation, Cuervo et al., 2016
Duvernay Reserves and Resources Report, Alberta Energy Regulator, www.aer.ca ,2016